MAGNETIC RESONANCE IN MEDICINE 10, 324–337 (1989)

Effects of Intravoxel Incoherent Motions (IVIM) in Steady-State Free Precession (SSFP) Imaging: Application to Molecular Diffusion Imaging

D. LE BIHAN,* R. TURNER,† AND J. R. MACFALL‡

Diagnostic Radiology Department, The Warren Grant Magnuson Clinical Center, Building 10, Room 1C660, and †Bioengineering and Instrumentation Branch, National Institutes of Health, Bethesda, Maryland 20892; and ‡General Electric Company, Medical Systems Group, P.O. Box 414, Milwaukee, Wisconsin 53201

Received August 17, 1988; revised November 9, 1988

A theoretical analysis of the effects of diffusion and perfusion in *s*teady-*s*tate *f*ree *p*recession (SSFP) imaging sequences sensitized to intravoxel incoherent motions by magnetic field gradients is presented and supported by phantom studies. The capability of such sequences to image diffusion and perfusion quickly was recently demonstrated. The possible residual effects of T_1 and T_2 in diffusion measurements are evaluated, as are the effects of the sequence design and the acquisition parameters (repetition time, flip angle, gradient pulses). It is shown theoretically and confirmed by experiments on phantoms that diffusion coefficients can be directly measured from SSFP images when large enough diffusion gradient pulses are used. © 1989 Academic Press, Inc.

INTRODUCTION

The effects of molecular diffusion in spin echoes in the presence of magnetic field gradients were demonstrated and analyzed in the 1950s (*1–3*). Stejskal and Tanner were then able to measure diffusion coefficients in liquids using strong gradient pulses added to a spin-echo sequence (*4*). In consequence, until recently, diffusion images have been generated using appropriate spin-echo sequences with additional gradient pulses to increase their sensitivity to diffusion (*5, 6*). Because other microscopic motions may occur *in vivo*, such as blood microcirculation, the diffusion imaging concept has been enlarged to *i*ntravoxel *i*ncoherent *m*otion (IVIM) imaging, which takes into account all possible random motion phenomena at the voxel scale (*6*). Diffusion and blood microcirculation imaging have appeared already very promising, allowing better tissue characterization than conventional MRI and demonstrating the capability of functional studies (*7*). However, the presence of the additional IVIM-probe gradient pulses in spin-echo sequences results in a long acquisition time to compensate for low signal levels (typically twice 8 min). Fast imaging techniques may thus prove to be useful, with appropriate sensitization to IVIM effects (*8*). Recently, the effects of diffusion or microcirculation in *s*teady-state *f*ree *p*recession (SSFP) sequences have been shown (*9–11*) and SSFP has been proposed to specifically image IVIMs (*9*). The use of SSFP sequences for MR imaging is not new (*12*), and extensive analyses of the dependence of the SSFP signals on the MR parameters in Fourier

0740-3194/89 $3.00

experiments (*12–14*) and MR imaging (*15*) have been published. Although diffusion effects in Fourier analyzed experiments using SSFP have been previously described (*16*), nothing has been published to our knowledge on such effects in SSFP imaging, where T_1 and T_2 spatial variations may interfere with diffusion measurements. We propose then to provide such an analysis and to validate it by comparing simulations obtained from the analysis with experimental data. This permits an optimization of the previously designed SSFP imaging sequence (*9*) to quantitatively image molecular diffusion.

THEORETICAL ANALYSIS

The SSFP Magnetization in the Presence of IVIMs

The equations for the steady-state magnetization obtained with a train of rf pulses regularly spaced (flip angle α along the x axis, repetition interval TR) have been well established (*12–14*). The different steps of the calculation will be summarized briefly in order to show how IVIM effects can be incorporated.

For a population of isochromatic spins (such as in a homogeneous voxel at location $\mathbf{r}$), the magnetization $\mathbf{M}(\mathbf{r}, t)$ after the n^{th} rf pulse is given by

$$\mathbf{M}_n(\mathbf{r}, t) = R(t)\mathbf{M}_n(\mathbf{r}, 0) + M_0(1 - e^{-t/T1})\hat{\mathbf{k}}, \qquad [1]$$

where $\hat{\mathbf{k}}$ is the unit vector associated to the z axis (direction of the main magnetic field) and $R(t)$ describes the precession of spins in the presence of magnetic fields and relaxation according to Bloch equations. The magnetization immediately following the n^{th} pulse is deduced from the magnetization at the end of the $(n-1)^{\text{st}}$ cycle by

$$\mathbf{M}_n(\mathbf{r}, 0) = P_x(\alpha) \cdot \mathbf{M}_{n-1}(\mathbf{r}, \text{TR}), \qquad [2]$$

where $P_x(\alpha)$ is the operator associated with the rf pulses. If relaxation effects can be neglected during the rf pulses, $P_x(\alpha)$ can be described by

$$P_x(\alpha) = \begin{bmatrix} 1 & 0 & 0 \\ 0 & \cos\alpha & \sin\alpha \\ 0 & -\sin\alpha & \cos\alpha \end{bmatrix}. \qquad [3]$$

The steady-state condition for the magnetization can be written as

$$\mathbf{M}_n(\mathbf{r}, 0) = \mathbf{M}_{n-1}(\mathbf{r}, 0) \equiv \mathbf{M}(\mathbf{r}, 0). \qquad [4]$$

Combining Eq. [1], [2] and [4] we obtain

$$\mathbf{M}(\mathbf{r}, 0) = M_0(1 - E_1)[P_x^{-1}(\alpha) - R(\text{TR})]^{-1}\hat{\mathbf{k}}, \qquad [5]$$

where $E_1 = \exp(-\text{TR}/T_1)$, and the magnetization $\mathbf{M}(\mathbf{r}, t)$ at any time between two successive rf pulses is

$$\mathbf{M}(\mathbf{r}, t) = M_0(1 - E_1)R(t)[P_x^{-1}(\alpha) - R(\text{TR})]^{-1}\hat{\mathbf{k}} + M_0(1 - e^{-t/T1})\hat{\mathbf{k}}, \qquad [6]$$

Let us now write explicitly the operator $R(t)$ in the rotating frame. It includes relaxation and magnetic field effects,

$$R(t) = \begin{bmatrix} e^{-t/T_2}\cos\Phi(\mathbf{r},t) & e^{-t/T_2}\sin\Phi(\mathbf{r},t) & 0 \\ -e^{-t/T_2}\sin\Phi(\mathbf{r},t) & e^{-t/T_2}\cos\Phi(\mathbf{r},t) & 0 \\ 0 & 0 & e^{-t/T_1} \end{bmatrix}, \quad [7]$$

where $\Phi(\mathbf{r}, t)$ is the dephasing acquired by isochromatic spins at location $\mathbf{r}$.

Let us consider now the presence of incoherent motions. There is a distribution of dephasings in each voxel, and $R(t)$ must be averaged in each voxel according to the theorem of the central limit:

$$\langle R(t)\rangle = \begin{bmatrix} e^{-t/T_2}\langle\cos\Phi(\mathbf{r},t)\rangle & e^{-t/T_2}\langle\sin\Phi(\mathbf{r},t)\rangle & 0 \\ -e^{-t/T_2}\langle\sin\Phi(\mathbf{r},t)\rangle & e^{-t/T_2}\langle\cos\Phi(\mathbf{r},t)\rangle & 0 \\ 0 & 0 & e^{-t/T_1} \end{bmatrix}. \quad [8]$$

On the other hand, in the presence of microscopic motions occurring inside each voxel, such as in the diffusion process, the positions of spins can be described by

$$\mathbf{r}(t) = \mathbf{r}_0 + \mathbf{u}(t), \qquad \text{with} \qquad \mathbf{u}^2 \ll \mathbf{r}_0^2, \quad [9]$$

where $\mathbf{r}_0$ is the fixed voxel location and $\mathbf{u}(t)$ the instantaneous displacement in the voxel.

The dephasing $\Phi(\mathbf{r}, t)$ can then be written as

$$\Phi(\mathbf{r}, t) = \Phi_{r_0}(t) + \Phi_u(t) \quad [10a]$$

with

$$\Phi_{r_0}(t) = \gamma \int_0^t \mathbf{G}\cdot\mathbf{r}_0\, dt \quad [10b]$$

$$\Phi_u(t) = \gamma \int_0^t \mathbf{G}\cdot\mathbf{u}\, dt, \quad [10c]$$

where we assume that field inhomogeneities can be described by an instantaneous linear gradient $\mathbf{G}$.

The average quantities in $\langle R(t)\rangle$ can now be rewritten as

$$\langle\cos\Phi(\mathbf{r},t)\rangle = \cos\Phi_{r_0}(t)\langle\cos\Phi_u(t)\rangle - \sin\Phi_{r_0}(t)\langle\sin\Phi_u(t)\rangle \quad [11a]$$

$$\langle\sin\Phi(\mathbf{r},t)\rangle = \cos\Phi_{r_0}(t)\langle\sin\Phi_u(t)\rangle + \sin\Phi_{r_0}(t)\langle\cos\Phi_u(t)\rangle. \quad [11b]$$

In the case of pure random incoherent motions, such as diffusion, parity considerations require that

$$\langle\sin\Phi_u(t)\rangle = 0 \quad [12a]$$

and taking into account the normalized phase distribution in the voxel $p(\Phi_u, t)$,

$$\langle\cos\Phi_u(t)\rangle = \int_0^{2\pi} \cos\Phi_u(t)p(\Phi_u, t)d\Phi_u \equiv A(t). \quad [12b]$$

Since $A(t) \leqslant 1$, the effects of IVIMs will be an attenuation of the signal. Finally, under the above assumptions, $R(t)$ can be written from Eqs. [8], [11], and [12]

$$\langle R(t)\rangle = \begin{bmatrix} e^{-t/T_2}A(t)\cos\Phi_{r_0}(t) & e^{-t/T_2}A(t)\sin\Phi_{r_0}(t) & 0 \\ -e^{-t/T_2}A(t)\sin\Phi_{r_0}(t) & e^{-t/T_2}A(t)\cos\Phi_{r_0}(t) & 0 \\ 0 & 0 & e^{-t/T_1} \end{bmatrix}. \quad [13]$$

It is now easy to see that the steady-state magnetization in the presence of IVIMs can be deduced from the classical equations by multiplying each term involving T_2 by an attenuation factor $A(t)$. This can be seen as an effective $T_{2_{\text{eff}}}$ effect, with $T_{2_{\text{eff}}} < T_2$, as commonly used in classic spin-echo experiments. In other words, the phase incoherence caused by transverse relaxation is enhanced by IVIMs in the presence of magnetic field gradients. This enhancement will be directly dependent on the phase dispersion in each voxel.

The steady-state magnetization can then be calculated from Eqs. [6] and [13] at any time t between two successive rf pulses,

$$M_x(t, r_0) = Q \sin\alpha E_2' A'[E_2 A_2 \sin\Phi_{r_0}(\text{TR} - t) + \sin\Phi_{r_0}(t)] \quad [14a]$$

$$M_y(t, r_0) = -Q \sin\alpha E_2' A'[E_2 A_2 \cos\Phi_{r_0}(\text{TR} - t) - \cos\Phi_{r_0}(t)] \quad [14b]$$

with

$$Q = \frac{M_0(1 - E_1)}{1 - E_1\cos\alpha - (E_1 - \cos\alpha)(E_2 A)^2 + E_2 A(E_1 - 1)(1 + \cos\alpha)\cos\Phi_{r_0}(\text{TR})}, \quad [14c]$$

where $E_1 = e^{-\text{TR}/T_1}$, $E_2 = e^{-\text{TR}/T_2}$, $E_2' = e^{-t/T_2}$, $A = A(\text{TR})$, $A' = A(t)$.

The equivalence between t and $(\text{TR} - t)$ in [14] results in the well-known fact that two signal formations can be observed in the presence of a inhomogeneous field, one just after each rf pulse (free induction decay (FID) or "Echo 1"), one just before each rf pulse ("Echo 2") (Fig. 1). The complex magnetization for Echo 1 (at $t = 0$) and Echo 2 (at $t = \text{TR}$) is then

$$M_+(0, r_0) = Q \sin\alpha[1 - E_2 A e^{-i\Phi_{r_0}(\text{TR})}] \quad [15a]$$

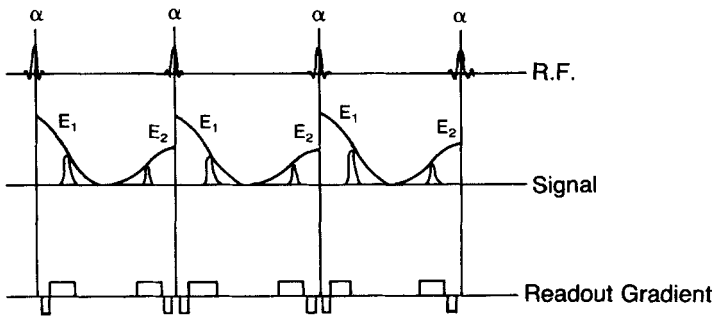

FIG. 1. Schematic diagram of SSFP. A train of regularly spaced rf pulses (flip angle α) produces a steady-state transverse magnetization. It results in two signal formations, one just after each pulse (Echo 1 or FID), the other immediately preceding each pulse (Echo 2). These two echo signal formations may be separately monitored for imaging by using gradient-recalled echoes.

$$M_+(\mathrm{TR}, r_0) = Q \sin\alpha[e^{i\Phi r_0(\mathrm{TR})} - E_2A]E_2A \quad [15b]$$

with $M_+(t, r_0) = M_y(t, r_0) + iM_x(t, r_0)$.

Similarly, the steady-state magnetization $M'_+(t, r_0)$ can be established in the case of phase alternated rf pulses (flip angle $(-1)^n\alpha$). One finds

$$M'_+(0, r_0) = (-1)^n Q' \sin\alpha[1 + E_2Ae^{-i\Phi r_0(\mathrm{TR})}] \quad [16a]$$

$$M'_+(\mathrm{TR}, r_0) = (-1)^n Q' \sin\alpha[e^{i\Phi r_0(\mathrm{TR})} + E_2A]E_2A \quad [16b]$$

with

$$Q' = \frac{M_0(1 - E_1)}{1 - E_1\cos\alpha - (E_1 - \cos\alpha)(E_2A)^2 - E_2A(E_1 - 1)(1 + \cos\alpha)\cos\Phi_{r_0}(\mathrm{TR})}. \quad [16c]$$

The IVIM Effects in SSFP Imaging

In an image acquired with an SSFP sequence, the dephasing Φ_{r_0} is mainly a result of the gradient pulses used for imaging. Both Echo 1 and Echo 2 can be monitored by sampling the signal immediately after or immediately before each rf pulse, or more exactly the gradient-recalled echo delayed or advanced in the cycle by a time-reversal readout gradient (Fig. 1). Depending on which echo (1 or/and 2) is monitored, different acronyms have been attached to such sequences (refocused FLASH, FAST, CE-FAST, GRASS, FISP, etc.). It appears from Eq. [10b] that the signal phase and amplitude will depend on the position r_0 of each voxel throughout the gradient. The result is a periodic variation of the signal amplitude across the image (*15*). This periodicity can be explained by an interference between Echo 1 and Echo 2 during the sampling window. It can be modulated by "crusher" gradient pulses which will destroy either the Echo 1 or the Echo 2. The periodicity can thus be forçed to be less than the voxel size and can no longer be seen. Using a similar approach, Zur *et al.* (*15*) calculated the signal intensity in a SSFP image under this image uniformity criterion. Taking IVIM effects into account, in the fashion mentioned above, i.e., by multiplying each term involving T_2 by an attenuation factor A, we find respectively for Echo 1 and Echo 2 signals, in the case of an imaging sequence involving a constant-phase rf pulse train, with an echo time TE, and sensitized to diffusion/perfusion by an additional gradient pulse (Figs. 2a and 2b),

$$S_1 = M_0 \frac{e^{-\mathrm{TE}/T_2}A(\mathrm{TE})\sin\alpha}{(1 + \cos\alpha)}\left\{1 - (E_1 - \cos\alpha)\left[\frac{1 - (E_2A)^2}{q}\right]^{1/2}\right\} \quad [17a]$$

$$S_2 = -M_0 \frac{e^{-\mathrm{TE}/T_2}A(\mathrm{TE})\sin\alpha}{(1 + \cos\alpha)E_2A}\left\{1 - (1 - E_1\cos\alpha)\left[\frac{1 - (E_2A)^2}{q}\right]^{1/2}\right\}, \quad [17b]$$

where

$$q = 1 - E_1^2(E_2A)^2 - 2E_1(1 - (E_2A)^2)\cos\alpha + (E_1^2 - (E_2A)^2)\cos^2\alpha \quad [17c]$$

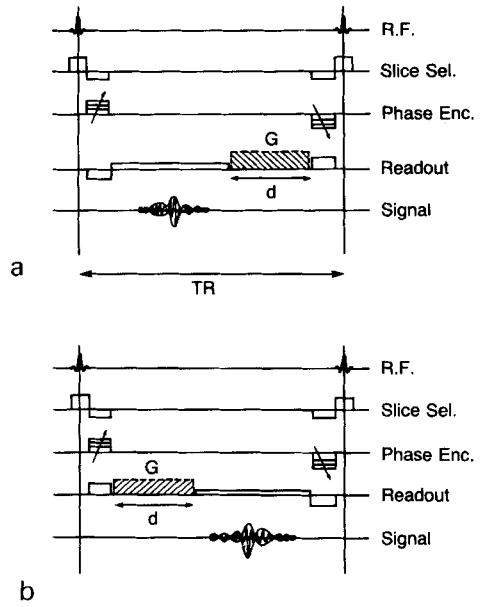

FIG. 2. SSFP imaging sequences can be sensitized to intravoxel incoherent motions by the presence of an additional gradient pulse (strength G, duration d). The configuration of the gradient pulses on the readout gradient axis is designed in such a way that the first echo (a) or the second echo (b) is monitored, while the other is destroyed. The result is an attenuation of the SSFP signal, as a function of the diffusion coefficient D, and the gradient pulse sequence (gradient factor b).

and, in the case of a phase-alternated pulse train,

$$S'_1 = S_1 \qquad [17d]$$

$$S'_2 = -S_2. \qquad [17e]$$

Equation [17] simplifies, when using $\alpha = 90°$, to

$$S_1 = M_0 e^{-\mathrm{TE}/T_2} A(\mathrm{TE}) \left\{ 1 - \left[\frac{E_1^2(1-(E_2A)^2)}{1-(E_1E_2A)^2} \right]^{1/2} \right\} \qquad [18a]$$

$$S_2 = -M_0 [e^{-\mathrm{TE}/T_2} A(\mathrm{TE})/(E_2A)] \left\{ 1 - \left[\frac{1-(E_2A)^2}{1-(E_1E_2A)^2} \right]^{1/2} \right\}. \qquad [18b]$$

Under the condition where $(E_2A)^2 \ll 1$, Eqs. [17] and [18] simplify further, and by using TE ≈ 0 for Echo 1 and TE $\approx$ TR for Echo 2,

$$S_1 \simeq M_0 \frac{(1-E_1)[1+E_1(E_2A)^2/2]}{1-(E_1E_2A)^2/2} \qquad [19a]$$

$$S_2 \simeq -M_0 \frac{(1-E_1^2)(E_2A)^2/2}{1-(E_1E_2A)^2/2}. \qquad [19b]$$

Equation [19a] shows that it is very difficult to separate or eliminate effects of T_1 and T_2 on Echo 1. In consequence, the effectiveness of Echo 1 for IVIM imaging will be very poor compared to that which can be expected from Echo 2 (Figs. 3 and 4).

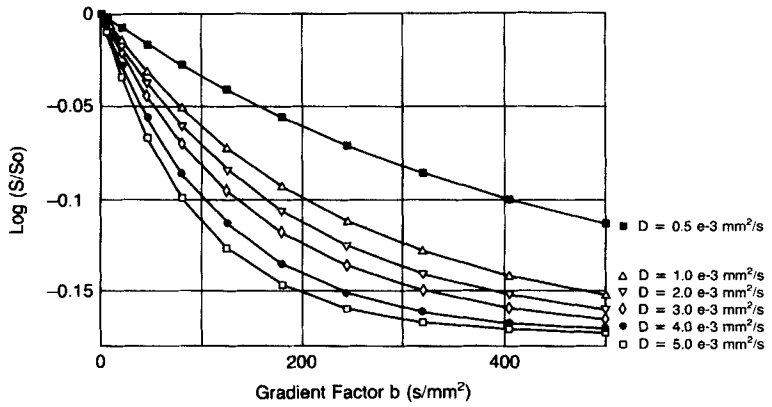

FIG. 3. Simulation of the evolution of the logarithm of the echo attenuation in an SSFP sequence using Echo 1 (TR = 80 ms, $\alpha = 90°$), as a function of the gradient factor b for different diffusion coefficients D in a standard sample of biological tissue ($T_1 = 400$ ms, $T_2 = 80$ ms). There is no simple relation with the diffusion coefficients D, although strong diffusion effects are present, due to the presence of residual T_1 and T_2 effects which cannot be avoided using an SSFP Echo 1 sequence. This shows that the use of Echo 1 SSFP sequences to measure diffusion is unfruitful.

This is entirely consistent with the well-known result that Echo 2 is also more sensitive to transverse relaxation (*12–15*). The sensitivity of Echo 2 to IVIMs can be expressed as $d(\log(S_2))/dA$, and we obtain from Eq. [19b]

$$d(\log(S_2))/dA = (2/A)[1 + (E_1E_2A)^2/(2 - (E_1E_2A)^2)]. \quad [20]$$

When IVIM effects become strong enough, the effects of T_1 and T_2 vanish:

$$\lim_{A \to 0} d(\log(S_2))/dA = 2/A. \quad [21]$$

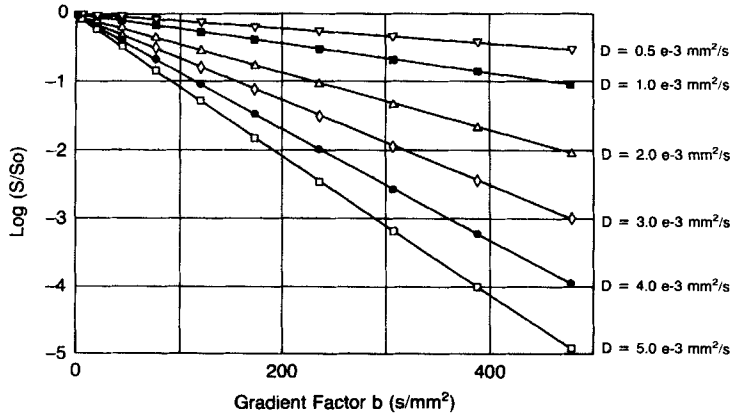

FIG. 4. Simulation of the evolution of the logarithm of the echo attenuation in an SSFP sequence using Echo 2 (TR = 80 ms, $\alpha = 90°$), as a function of the gradient factor b for different diffusion coefficients D in a standard sample of biological tissue ($T_1 = 400$ ms, $T_2 = 80$ ms). There is a direct relation between the slope of the curves and the diffusion coefficients D, suggesting the capability of Echo 2 SSFP sequences for diffusion measurements.

Quantitative imaging of IVIMs using an SSFP Echo 2 sequence thus appears to be possible (Fig. 4).

Application to Free Molecular Diffusion

Diffusion may be described by the probability $P(\mathbf{u}, t)$ that molecules will have a displacement $\mathbf{u}$ during a time interval t (*17*). In the case of the free Brownian diffusion, this probability is

$$P(\mathbf{u}, t)d\mathbf{u} = (4\pi Dt)^{-3/2}\exp[-\mathbf{u}^2/(4Dt)]d\mathbf{u}. \quad [22a]$$

This corresponds to a Gaussian distribution for $\mathbf{u}$, the mean of which is zero and the variance $2Dt$. In a given direction, i.e., the direction of the gradient $\mathbf{G}$,

$$P(u, t)du = (4\pi Dt)^{-1/2}\exp[-u^2/(4Dt)]du. \quad [22b]$$

The relation between displacements and dephasings is given by Eq. [10c]. A Fokker–Planck equation may now be derived using the phase angle as the independent variable. From this it is easily shown that the distribution of dephasings $p(\Phi_u, t)$ will also be a Gaussian distribution,

$$p(\Phi_u, t) = (2\pi\sigma^2)^{-1/2}\exp[-\Phi_u^2/(2\sigma^2)]d\Phi_u, \quad [23a]$$

with a variance

$$\sigma^2 = \langle\Phi_u^2\rangle = 2D\int_0^t \mathbf{k}^2 dt, \quad [23b]$$

where

$$\mathbf{k} = \gamma\int_0^t \mathbf{G}dt. \quad [23c]$$

In the case of a Gaussian distribution centered at 0 it is generally true that $\langle\cos x\rangle = \exp(-\sigma^2/2)$. Thus we obtain for molecular diffusion from Eqs. [12b] and [23]

$$A = \exp(-b\cdot D), \quad [24a]$$

where D is the diffusion coefficient and b a gradient factor defined by

$$b = \int_0^t \mathbf{k}^2 dt. \quad [24b]$$

Relation [21] then becomes

$$\lim_{b\to\infty} d(\log(S_2))/db = -2D. \quad [25]$$

This means that the sensitivity to diffusion will be twice that expected from the gradient factor b as calculated for a given cycle (TR) or that the diffusion effect will be that which would be obtained from two successive cycles. In other words, the SSFP sequence can be considered, under these conditions, as a spin-echo sequence with a TE echo time, where TE = 2TR, as far as diffusion effects are concerned. This is in perfect agreement with the result obtained by Kaiser *et al.* (*16*) considering fast diffusion. Indeed the condition is $(E_1E_2A)^2 \ll 1$; i.e., there is only a negligible amount of

residual signal following a given rf pulse after $t > 2TR$, due to T_1, T_2, or diffusion effects, so that multiple echo paths do not have to be considered.

COMPUTER SIMULATIONS

In order to evaluate diffusion effects in SSFP imaging, we have performed computer simulations of Eq. [17], or more exactly of $\log(S)$ as a function of the gradient factor b. The first purpose was to determine how the acquisition parameters (flip angle α, repetition time TR) affect the SSFP sensitivity to diffusion. This enables an optimization of these acquisition parameters taking into account signal-to-noise considerations. The second purpose was to see how diffusion measurements can be obtained from SSFP sequences with a reasonable rejection of T_1 and T_2 residual effects. Simulations have been done in the case of an SSFP sequence monitoring Echo 2 (Fig. 2b), in which diffusion effects have been shown to be much more obvious than those in Echo 1.

Effects of Flip Angle and Repetition Time

The plot of $\log(S)$ as a function of b for different values of the flip angle α or the repetition time TR was obtained for a "standard" sample whose MR parameters were close to those expected for biological tissues (T_1 = 400 ms, T_2 = 80 ms, $D = 2.5 \times 10^{-3}$ mm^2/s). The sensitivity to diffusion is given by the slope of this plot.

As shown in Fig. 5, the sensitivity of SSFP imaging to diffusion is virtually independent of the flip angle. It follows that α must be chosen only according to signal-to-noise ratio considerations.

As shown in Fig. 6, the sensitivity of SSFP imaging to diffusion shows very little dependence on the repetition time, as long as TR is not too short compared to T_1 and T_2. Indeed, the effect of using short TR values is not to change the sensitivity of

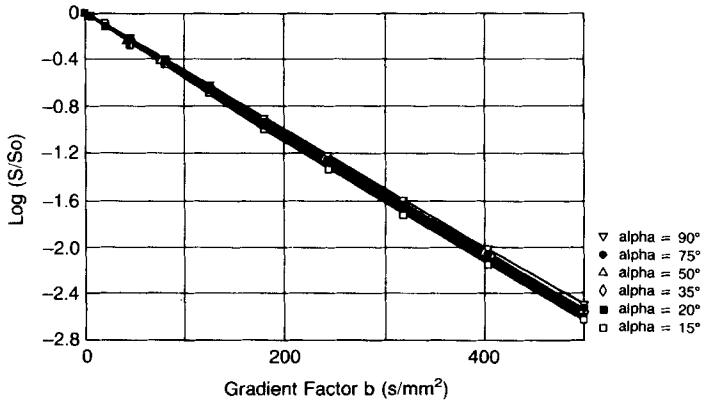

FIG. 5. Simulation of the evolution of the logarithm of the Echo 2 attenuation as a function of the gradient factor b for different flip angles (TR = 80 ms) in a standard sample of biological tissue (T_1 = 400 ms, T_2 = 80 ms, $D = 2.5 \times 10^{-3}$ mm^2/s). The effect of the flip angle appears negligible when its value is not too small. This allows the flip angle to be optimized in the IVIM SSFP sequence according to signal-to-noise ratio considerations.

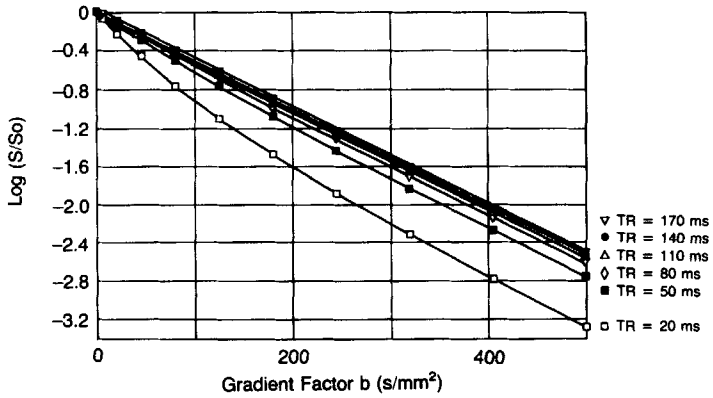

FIG. 6. Simulation of the evolution of the logarithm of the Echo 2 attenuation as a function of the gradient factor b for different TR values ($\alpha = 90°$) in a standard sample of biological tissue ($T_1 = 400$ ms, $T_2 = 80$ ms, $D = 2.5 \times 10^{-3}$ mm^2/s). The effect of TR on the slope of this curve (which gives the diffusion coefficient) can be considered negligible when TR is not too short (compared to T_1 and T_2). This effect leads to a compromise, the signal being smaller when TR is increased.

SSFP to diffusion, but to increase the value of the gradient factor b at which T_1, T_2, or TR effects become negligible, i.e., where the slope of the plot becomes constant and related only to the diffusion coefficient. The value of TR at which T_1 and T_2 effects can be considered negligible can be quantitatively evaluated by checking the assumption that $(E_1E_2A)^2 \ll 1$. From Eqs. [20] and [24], it appears that

$$d(\log(S))/db = -2D[1 + \beta], \qquad [26]$$

where

$$\beta = (E_1E_2A)^2/[2 - (E_1E_2A)^2]. \qquad [27]$$

According to the desired value for β, the minimum TR can be calculated from Eq. [27], with $\alpha = 90°$, by

$$\mathrm{TR} > T_1 \cdot T_2/(T_1 + T_2)\{\log A - \tfrac{1}{2}\log[2\beta/(1 + \beta)]\}. \qquad [28]$$

With $T_1 = 400$ ms, $T_2 = 80$ ms, we obtain

$$\text{for } \beta = 0.1, \qquad \mathrm{TR\,(ms)} > 56.8 - 66.6\,(\mathrm{bD})$$

$$\text{for } \beta = 0.01, \qquad \mathrm{TR\,(ms)} > 131 - 66.6\,(\mathrm{bD}).$$

This limitation on TR will lead to a compromise with signal-to-noise ratio considerations, the Echo 2 SSFP signal becoming smaller when TR is increased (*15*). There is of course a technical limit to the shortness of TR, since the strength of the diffusion gradient pulse is hardware limited, and thus its duration must be extended to provide sufficient diffusion sensitization.

Effects of T_1 and T_2

Similarly, rejection of T_1 or T_2 residual effects can be obtained by using values of b which are sufficiently large, as shown in Fig. 7, to limit β in Eq. [26]:

$$b > -\{\tfrac{1}{2}\log[2\beta/(1 + \beta)] + \mathrm{TR}(T_1 + T_2)/(T_1 \cdot T_2)\}/D. \qquad [29]$$

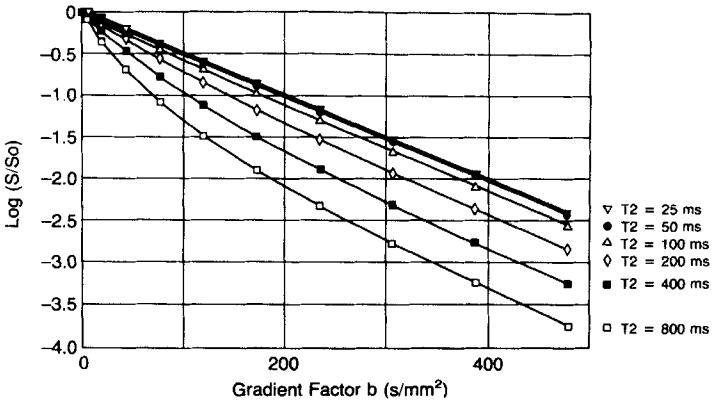

FIG. 7. Simulation of the evolution of the logarithm of the Echo 2 attenuation as a function of the gradient factor b for different T_2 values (TR = 80 ms, $\alpha = 90°$) in a standard sample of biological tissue (T_1 = 3000 ms, $D = 2.5 \times 10^{-3}$ mm^2/s). The effect of T_2 on the diffusion coefficient which would be measured from the slope of these curves appears negligible when using large b values, i.e., when using large enough diffusion gradient pulses.

With T_1 = 400 ms, T_2 = 80 ms, TR = 80 ms, and $D = 2.5 \times 10^{-3}$ mm^2/s, we obtain

$$\text{for } \beta = 0.1, \qquad b > -139 \text{ s/mm}^2,$$

i.e., the condition is already satisfied with $b = 0$,

$$\text{for } \beta = 0.01, \qquad b > 304 \text{ s/mm}^2,$$

a condition which can be reached with very strong gradient pulses, but which will decrease dramatically the signal level, according to Eq. [19b].

A good compromise would be to use b values as large as 200 s/mm^2, so that the residual T_1 and T_2 contamination β would be less than 1.7% using previous values for T_1, T_2, TR, and D. According to Eq. [29], this contamination will be less for smaller T_1 or T_2 values and more for larger T_1 or T_2 values.

Under these conditions, diffusion images could be obtained from two SSFP Echo 2 images differently sensitized to diffusion so that

$$D(x, y) = \log[S_0(x, y)/S_1(x, y)]/(b_1 - b_0), \qquad [30]$$

where b_0, b_1 should be larger than 200 s/mm^2.

Figure 8 shows that the slope of the plot is then effectively given by the diffusion coefficient with negligible T_2 effects, as long as values used for D and T_2 are in a range expected in biological tissues.

EXPERIMENTAL STUDIES

In order to validate the above theoretical analysis, a phantom study was performed. All measurements were obtained on a 1.5-T whole-body MR imager (Signa, General

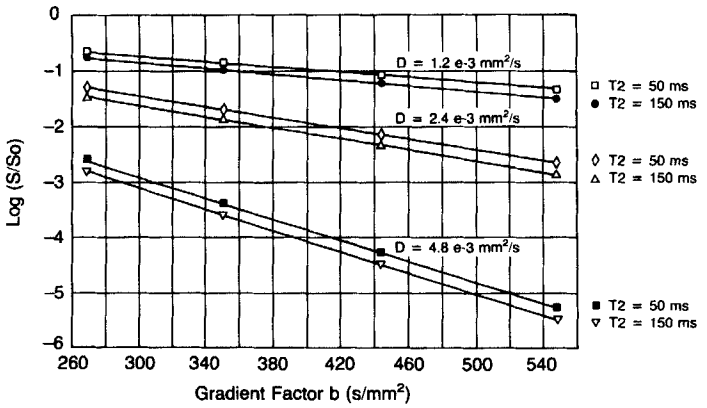

FIG. 8. Simulation of the evolution of the logarithm of the Echo 2 attenuation as a function of the gradient factor b ($b > 200$ s/mm^2) for different samples of biological tissues ($T_1 = 400$ ms, $T_2 = 50$ and 150 ms) with different diffusion coefficients corresponding to those expected in normal tissues (1.2×10^{-3} mm^2/s), in liquid structures, such as in cysts or edema (2.4×10^{-3} mm^2/s), and in the presence of high perfusion (pseudo-diffusion) (4.8×10^{-3} mm^2/s). The diffusion coefficients which would be measured from the slope of these curves in real situations are not affected by T_2 effects, as long as strong enough gradient pulses are used.

Electric). The phantom consisted of separate tubes containing acetone, water, and a polyacrylamide gel doped with copper sulfate (20 mM/liter) allowing a broad range of diffusion coefficients, T_1, and T_2 to be covered. The diffusion coefficient was measured in each tube from diffusion MR images using spin-echo sequences sensitized with additional gradient pulses (*6*). These measurements were done just before the use of the SSFP sequence to minimize possible effects of temperature variations. The position of each tube inside the magnet was strictly maintained between the spin-echo and the SSFP experiments to eliminate the effect of possible nonuniformity of the gradient pulses through the imaged slice. Approximate values of T_1 and T_2 were also obtained using spin-echo sequences. The results are given in Table 1.

The SSFP Echo 2 sequence was sensitized to diffusion by an additional pulse gradient (strength G, duration d) on the readout direction in a design previously published (*9*) (Fig. 2b). The gradient factor b calculated from Eq. [24b] for such an isolated diffusion gradient is

$$b = \gamma^2 G^2 d^2 (\mathrm{TR} - 2d/3 - t_0), \qquad [31]$$

where t_0 is the time interval between the rf pulse and the diffusion gradient.

TABLE 1

Magnetic Resonance Parameters of the Phantoms (Measured from Spin-Echo Sequences)

	Water	Gel ($CuSO_4$, 20 mM/liter)	Acetone
T_1 (ms)	3200	179	4500
T_2 (ms)	1919	92	1082
D ($\times 10^{-3}$ mm^2/s)	2.35	2.00	4.88

TABLE 2

Gradient Factor b (Numerically Calculated using Eq. [24b] and Including All Gradient Pulses Present on the Readout Axis, as Shown in Fig. 2b)

G (G/cm)	b (s/mm^2)
0.3	54.4
0.4	90.7
0.5	136.4
0.6	191.4
0.7	255.6
0.8	329.1
0.9	412.0
1.0	504.0

Indeed, because of the presence of cross-terms in the development of Eq. [24b] the other gradient pulses set on the readout axis may have a nonnegligible role and should be taken into account at least for small G values. Under these conditions, b should be calculated numerically from Eq. [24b].

SSFP Echo 2 images were acquired with this sequence (TR = 80 ms, TE = 70 ms, $\alpha = 90°$, four excitations, 128 × 256 resolution matrix, corresponding to 41 s of acquisition time). The duration d of the diffusion gradient was 45 ms, maximum value compatible with TR and TE used, and kept constant in all acquisitions. Acquisitions were obtained with different gradient strengths G from 0.3 to 1 G/cm (the maximum value available in our system), corresponding to b values from 54 to 504 s/mm^2 (Table 2).

The signal in each tube was measured from the images using ROIs and plotted against calculated b values (Fig. 9). The expected signal was calculated with Eq. [17b] in its complete form, using the values of T_1, T_2, and D measured from spin-echo sequences, and plotted on the same graph for comparison. As shown in the figure, the agreement was found to be excellent, demonstrating the validity of the theory described above, which contains no free parameters.

CONCLUSIONS

The effects of diffusion in SSFP imaging sequences have been experimentally demonstrated and shown to be consistent with a theory which assumes that diffusion in the presence of a magnetic field gradient produces an incoherent dephasing similar to spin–spin relaxation. When the second echo in the SSFP sequence is used to generate the image, the sensitivity to diffusion is considerably enhanced. The residual effects of spatial variations in T_1 and T_2 may then be minimized by using sufficiently large diffusion gradients, such that only two cycles need to be considered in the formation of the echo. It is worth noting that a sequence using a balanced bipolar diffusion gradient can also produce interesting diffusion contrast. However, considerably larger values of field gradient are required to obtain useful information, as we have observed in preliminary experiments. The speed with which diffusion and perfusion images

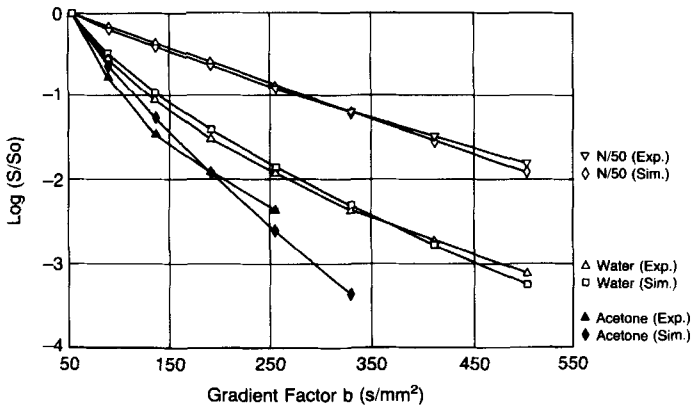

FIG. 9. Correlation between simulation (sim) and experiment (exp). The measured evolution of the logarithm of the Echo 2 attenuation is reported as a function of the gradient factor b (calculated from the gradient pulse sequence from Eq. [24b]) for a phantom made of three bottles containing respectively acetone, water, and a polyacrylamide gel doped with copper sulfate (N/50 or 20 mM/liter). On the same plot, the theoretical attenuation is given for the same phantom according to T_1, T_2, and D values, as measured using spin-echo sequences (Table 1), so that there is no free parameter. The agreement was found to be excellent.

may be obtained with this technique recommends it for clinical use, since artifacts caused by patient motion are likely to be far less severe than those with a spin-echo technique.

ACKNOWLEDGMENT

The authors gratefully acknowledge the In-Vivo NMR Center, NIH, for its support in experimental studies.

REFERENCES

1. E. L. HAHN, *Phys. Rev.* **80,** 580 (1950).
2. H. Y. CARR AND E. M. PURCELL, *Phys. Rev.* **94,** 630 (1954).
3. H. C. TORREY, *Phys. Rev.* **104,** 563 (1956).
4. E. O. STEJSKAL AND J. E. TANNER, *J. Chem. Phys.* **42,** 288 (1965).
5. D. G. TAYLOR AND M. C. BUSHELL, *Phys. Med. Biol.* **30,** 345 (1985).
6. D. LE BIHAN, E. BRETON, D. LALLEMAND, E. CABANIS, AND M. LAVAL-JEANTET, *Radiology* **601,** 401 (1986).
7. D. LE BIHAN, E. BRETON, D. LALLEMAND, M. L. AUBIN, J. VIGNAUD, AND M. L. LAVAL-JEANTET, *Radiology* **168,** 497 (1988).
8. R. TURNER, *in* "Cerebral Blood Flow" (A. Rescigno and A. Boicelli, Eds.), p. 245, Plenum, New York, 1988.
9. D. LE BIHAN, *Magn. Reson. Med.* **7,** 346 (1988).
10. S. PATZ AND R. C. HAWKES, *Magn. Reson. Med.* **3,** 140 (1986).
11. S. PATZ, M. S. ROOS, AND S. WRONG, "Proceedings, 6th Annual Meeting SMRM, Montreal," p. 425, 1987.
12. W. S. HINSHAW, *J. Appl. Phys.* **47,** 3709 (1976).
13. R. R. ERNST AND W. A. ANDERSON, *Rev. Sci. Instrum.* **37,** 93 (1966).
14. R. FREEMAN AND H. D. W. HILL, *J. Magn. Reson.* **4,** 366 (1971).
15. Y. ZUR, S. STOKAR, AND P. BENDEL, *Magn. Reson. Med.* **6,** 175 (1988).
16. R. KAISER, E. BARTHOLDI, AND R. R. ERNST, *J. Chem. Phys.* **60**(8), 2966 (1974).
17. J. E. TANNER AND E. O. STEJSKAL, *J. Chem. Phys.* **49,** 1768 (1968).